2017

Numerical Simulation of Gas Separation by Hollow Fiber Membrane

Alaa K. Hakim
Lehigh University

NUMERICAL SIMULATION
OF
GAS SEPARATION BY HOLLOW FIBER MEMBRANE

By

Alaa K. Hakim

A Thesis
Presented to the Graduate and Research Committee
Of Lehigh University
In Candidacy for the Degree of
Master of Science
In
Mechanical Engineering and Mechanics

Lehigh University
Spring 2017 Semester
May 2017

COPYRIGHT PAGE

CERTIFICATION OF APPROVAL

This thesis is accepted and approved in partial fulfillment of the requirements for the Master of Science.

_____

Date

_____

Thesis Advisor, Dr. Alparslan Oztekin

_____

Chairperson of Department, Dr. Gary Harlow

CONTENTS

LIST OF FIGURES

LIST OF TABLES

ACKNOWLEDGMENT

Firstly, I would like to thank my thesis advisor Professor Oztekin for his encouragement, advice, and assistance.

I thank my colleague Dr. Ali Anqi. Ali made me interested in this topic and inspired me to conduct research. In addition, I would like to thank my colleague Mustafa Usta for generously helping me to overcome all problems and obstacles that I faced.

I would like to thank my sponsor HCED (The Higher Committee for Education Development in Iraq) for their sponsorship and support, despite all the challenges and difficulties faced my country, Iraq. Also, I would like to thank the Ministry of Oil (MOO), and Missan Oil Company (MOC) for their support scientifically and financially.

Moreover, I must express my very profound gratitude to my parents (Kadhim H. Buraa, Nahlah M. Kadhim), my brothers and sister (Mohammed with his wife Ruaa, his son Jaafer, Hussain, Zahraa, Fatima) for their endless support and encouragement.

Finally, I would like to thank with appreciation my wife (Hiba Abd Ali) and my beloved children (Abbas, Retaj) for their generous love and encouragement throughout the academic life.

Author
Alaa K Hakim

NOMENCLATURE

A_{m}	surface area $[m^2]$	x_i	position vector
C	concentration $[mol/m^3]$	α	mass selectivity [-]
D_h	hydraulic diameter $[m]$	θ	angle $[degree]$
D	diffusion coefficient $[m^2/s]$	κ	membrane flux parameter [-]
e	the discrete velocity vector	μ	dynamic viscosity $[kg/m \cdot s]$
fr_i	friction factor in an inline geometry	ν	kinematic viscosity $[m^2/s]$
fr_s	friction factor in a staggered geometry	ρ	density $[kg/m^3]$
fr	the average friction factor	τ_g	mass relaxation time
h	height $[m]$	ω	specific dissipation rate $[1/s]$
h_m	mass transfer coefficient $[m/s]$	V_w	suction rate $[m/s]$
J	molar flux $[mol/m^2]$		
l	membrane thickness $[m]$		
L	computational domain length $[m]$		
m	mass flux $[kg/m^2 \cdot s]$		
M	molecular weight $[g/mol]$		
N	mole fraction [-]		
N_m	bulk mole fraction [-]		
p	pressure $[Pa]$		
Δp_L	pressure drop $[Pa]$		
Δp	pressure difference $[Pa]$		
A	permeance $[mol/m^2 \cdot s \cdot Pa]$		
$\ddot{A}$	permeability $[mol/m \cdot s \cdot Pa]$		
Re	Reynolds number [-]		
S	spacing $[m]$		
Sc	Schmidt number [-]		
$\dot{m}$	mass flow rate per unit area [kg/$m^2 \cdot s$]		
Sh	Sherwood number [-]		
t	time $[s]$		
u_i	flow velocity vector		
U	average velocity $[m/s]$		

Subscripts and Superscripts

a and b	species: CO_2 or CH_4	w	properties at the membrane surface
i and j	index notation	t	eddy properties
CH_4	properties of CH_4	CO_2	properties of CO_2
m	discrete direction	a/b	the ratio of properties of a to properties of b
tot	total properties		

ABSTRACT

Numerical analyses are performed for reverse osmosis gas separation modules consisting of hollow fiber membranes. Computational fluid dynamic simulations are conducted to study steady state flow and mass transport in three-dimensional separation modules. The fluid is a binary mixture of carbon dioxide (CO_2) and methane (CH_4). The mixture flows in a direction parallel to the membrane axis. The separation module consists of an inline and a staggered arrangement of hollow fibers with two different spacing. Equations governing the laminar flow of binary mixture, Navier-Stokes equation, and mass transport equations, are solved for Reynolds number of 1000, 1500, and 2000. The hollow fiber membrane is treated as a permeable, functional surface, where the mass flux of the species is computed as a function of local concentration, local partial pressures, the permeability, and the selectivity of the membrane. Flow and concentration field inside the module are characterized and the suction rate and concentration along surfaces of membranes are determined. Membrane flux performance is determined for the inline and the staggered configuration at all flow rates considered. Sherwood number of hollow fiber membranes is calculated for each configuration and spacing at all flow rates. It is shown here that area averaged Sherwood number asymptotes to a constant value away from the inlet. Sherwood number increases in both configurations as flow rate is increased and it decreases in both configurations as the spacing decreases. Merit number that compares the performance of different modules is introduced. The results show that modules consisting arrays of hollow fiber membranes in the staggered arrangement perform better than those with the inline arrangement at all values of spacing and flow rates considered in this study.

This study aids in designing and optimizing gas separation modules consisting of hollow fiber membranes.

1. INTRODUCTION

Natural gas is considered one of the important fossil fuel. It is found in the deepest layers of the earth and it is typically a side product of oil production. The demand for natural gas has been significantly increased recently. According to EIA (U.S. Energy Information Administration), the world utilization of natural gas has been increasing 4% annually; the usage is expected to reach 73% of the total needs for natural gas by 2040 for power production and industrial usage [19]. Natural gas contains several chemical compounds: CO_2, N_2, CH_4, water vapor, and H_2S. Compounds such as CO_2, N_2, water vapor, and H_2S are considered as impurities. These impurities could affect the pipelines adversely; causing corrosion and cracking. There are even health and safety concerns with CO_2 impurities in natural gas [21]. Membrane separation technology is applied for various industrial processes [10]. Reversible osmosis membrane separation is used to separate the impurities from natural gas.

There are various types of design for reversible osmosis membrane modules. Spiral wound membrane and hollow fiber membrane modules are two most common types. Hollow fiber membrane modules can be designed with the cross flow or parallel flow configurations. In the present study, an investigation of hollow fiber membrane characteristics and performance in a parallel flow model is studied with different spacing. The separation module design considered in this study is close to the one used in typical industrial applications for gas separation.

There are several investigations to study flow characteristics in gas separation modules. Few studies considered spacers in the feed channels to promote momentum mixing and support membranes. Saeed et al. [16] investigated flow structures in a feed

channel containing spacer with different spacing and arrangement. Saeed and his co-workers considered a three-dimensional feed channel in their study. They demonstrated that the mass transfer coefficient is similar in all cases even though the magnitude of shear stress along the surface of the membrane differs. Mojab et al. [14] conducted numerical and experimental studies to examine flow profiles in a feed channel filled with spacers and surrounded by spiral-wound membranes. They conducted transient simulations by utilizing turbulence model for a range of Reynolds number from 100 to 1000. They showed that the flow is steady for Reynolds number up to 200 and becomes oscillatory for Reynolds number greater than 250. Shakaib et al. [18] investigated the effect of spacers in a spiral wound membrane module. They reported that geometrical parameter of spacers such as thickness and the angle of attack profoundly influences the level of wall shear rates and the mass transfer coefficient. While Koutsou et al. [12] introduced a novel retentate-spacer design in order to eliminate the "dead-flow" zones that cause a reduction in mass transfer. The minimization of the contact area between spacers and membrane surfaces results in high shear stress and mass transfer rate along the membrane surface.

Karod et al [9] investigated the effect of the arrangement of spacers on pressure drop in a rectangular channel bounded by membranes. They observed that the symmetric spacers result in a uniform shear rate along the surface of membranes and high-pressure drop across the channel, while the asymmetric spacers cause lower pressure drop and non-uniform distribution wall shear rate along the surface of membranes. Fimbres-Weihs et al [7] investigated effects of a spacer configuration and the flow rate of the pressure drop and the mass transfer coefficient. They used an empirical relation to calculate the mass transfer coefficient, and the membrane wall was treated as the impermeable surface. Several

researchers treated the membrane surface as a permeable surface and considered the mass transport. Vinther et al [20] modeled the hollow fiber membrane for ultrafiltration process. Marocs et al [13] performed a transient simulation for a 2D model of hollow fiber membrane in an ultrafiltration system. Their results showed that the pressure drop is significantly influenced the concentration polarization. Anqi et al [4] conducted a three-dimensional computational study for a desalination process for a wide range of flow rates. Their desalination module contains a net of spacers in the feed channels. They treated the membrane surface as a permeable wall. Their results showed that the membrane performance is better at higher flow rates also that the arrangement of spacers influences the membrane performance significantly.

Alkhamis et al. [1] introduced a new mass flux model for a gas separation process via a reversible osmosis membrane module. The mass flux of species is determined based on the local pressure, concentration, permeability, and selectivity of the membrane. Alkhamis et al. [1] studied flow and mass transport in a spiral wound membrane module containing spacers. They proved that the spacers enhance the membrane function significantly. They claimed that the introducing of spacers in a feed channel should be an important part of the design of a separation system by a membrane. Alrehili et al. [3] conducted computational fluid dynamics simulations are conducted for a binary mixture of carbon dioxide (CO_2) and methane (The membrane module considered include a bank of hollow fiber membranes with two different arrangements: an inline and a staggered. Alrehili et al. [3] treated the membrane surface as a functional surface where the species mass flux and concentration are calculated as a function of partial pressures, and the membrane permeability and selectivity. They demonstrated that cross flow configuration

created in the bank of hollow fiber membranes induces a better mixing and as a result, it enhances membrane flux performance and improves the overall separation process. Moreover, they proved that staggered arrangements perform better than inline arrangements.

In this study, computational fluid dynamics simulations are conducted in a three-dimensional gas separation module by utilizing CFX Steady state flow and concentration field is characterized by the binary mixture of carbon dioxide (CO_2) and methane (CH_4) flowing through a bank of hollow fiber membranes. Axial flow configuration in the bank of hollow fibers is considered for three different values of flow rates. Hollow fiber membranes are arranged in an inline and a staggered configuration with two values of the spacing of fibers. Navier-Stokes and diffuse transport equations of the membrane are numerically solved for laminar flow binary mixture in the feed channel. The membrane is treated as a functional surface, where the mass flux of each species is computed based on the local partial pressures, the permeability, and the selectivity of the membrane. The study is to examine the effect of arrangement and spacing of hollow fibers the membrane flux performance in a gas separation module.

2. MATHEMATICAL MODEL

2.1 Geometry

A steady state flow simulations are conducted in a three-dimensional hollow fiber membrane module. The primary flow is parallel to the axis of hollow fiber membranes. Figure 1 depicts the schematic the three-dimensional computational domain containing an array a staggered arrangement and an inline arrangement of hollow fibers. The diameter of the membrane is *d* and the spacing between two adjacent hollow fiber membranes is *S*. Both arrangements are designed with two different spacing: *S/d = 1.1* and *S/d = 1.25*. The hydraulic diameter is calculated for each case based on an infinite number of fibers. *L/Dh = 40* is chosen for design the inline cases, while for the staggered cases *L/Dh* is 75, where *L* is the length of the module. Table 1 shows the geometry design criteria for all cases based on their hydraulic diameter.

	Inline		**Staggered**	
	S/d = 1.25	**S/d = 1.1**	**S/d =1.25**	**S/d = 1.1**
D_h	0.000989	0.00054	0.000723	0.000334
L/D_h	40	40	75	75

Table 1: Geometry length design criteria for inline and staggered cases

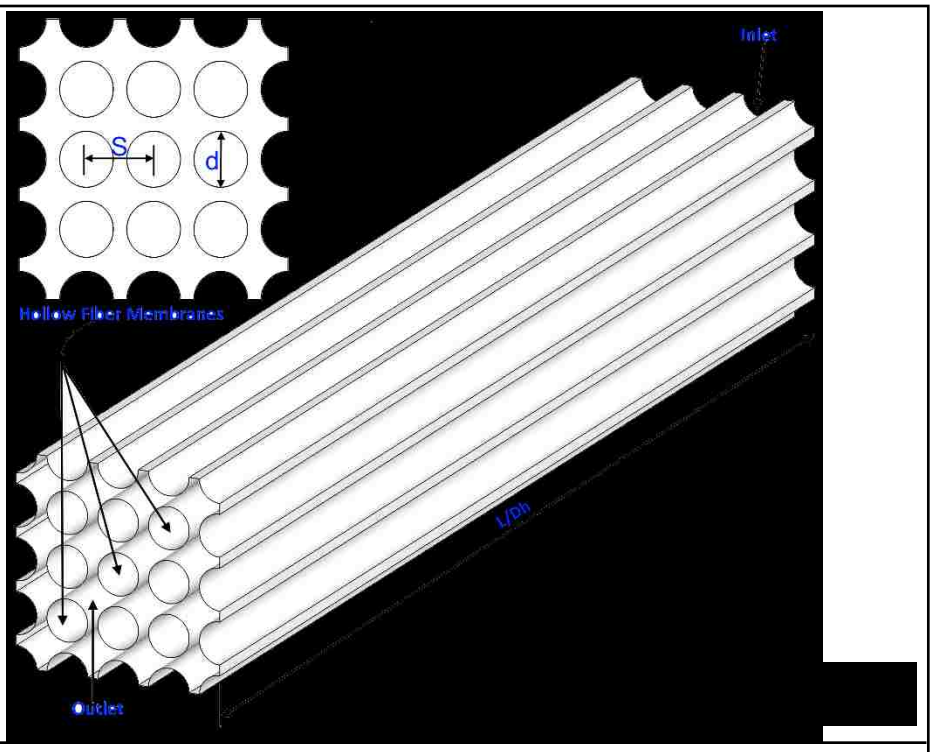
Inlet
S
d
Hollow Fiber Membranes
L/Dh
Outlet

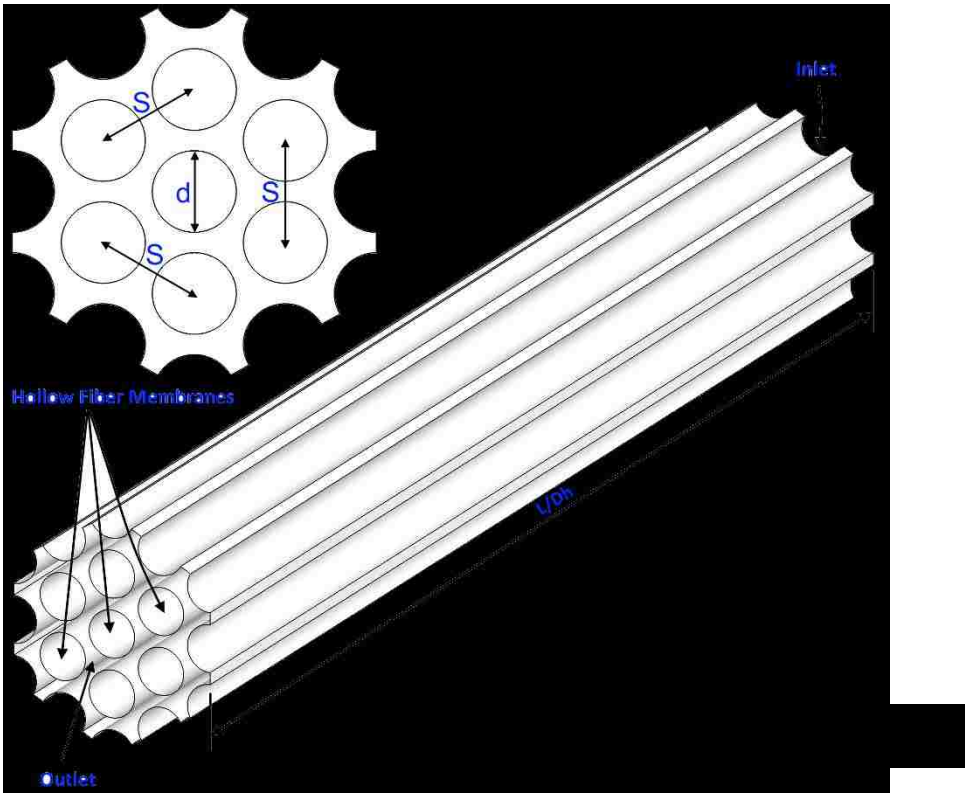
Inlet
S
d
S
S
Hollow Fiber Membranes
L/Dh
Outlet

2.2. Governing Equations

Steady state simulations are conducted in a three-dimensional feed channel for Reynold numbers: *Re = 1000, 1500,* and *2000*. The Reynolds number is defined as $Re = UD_h/\upsilon$, where U is the average fluid velocity at the inlet, D_h is the hydraulic diameter, and υ is the kinematic viscosity. The mixture properties are assumed to be constant and the diffusion coefficient is considered to be independent of the mixture concentration. Laminar model is utilized for the range of Reynolds numbers considered [15], [8]. Equations governing the fluid motion is Navier-Stokes equation as described below.

Conservation of mass:

$$\frac{\partial u_i}{\partial x_i} = 0, \tag{1}$$

Conservation of momentum:

$$\frac{\partial u_i}{\partial t} + u_j \frac{\partial u_i}{\partial x_j} = -\frac{1}{\rho}\frac{\partial p}{\partial x_i} + \upsilon \frac{\partial}{\partial x_j}\left(\frac{\partial u_i}{\partial x_j}\right), \tag{2}$$

Where j is the summation index; $i = 1, 2,$ and 3 for three-dimensional flows; $u_1 = u$, the stream-wise velocity; $u_2 = v$, span-wise velocity; $u_3 = w$, cross-wise velocity. Likewise, $x_1 \equiv x$ is the stream-wise direction; $x_2 \equiv y$ is the span-wise direction; $x_3 \equiv z$ is the cross-wise direction; t is time, P is the pressure; ν is the kinematic viscosity ($\nu = \mu/\rho$); ρ is the density of the mixture (i.e. $\rho = \rho_a + \rho_b$), where ρ_a and ρ_b are the density of species "*a*" and "*b*", respectively. The density of the mixture is assumed constant.

The mass transfer of the species "*a*" is governed by the mass transport equation:

$$\frac{\partial CN_a}{\partial t} + u_j \frac{\partial CN_a}{\partial x_j} = \frac{\partial}{\partial x_j}\left(D \frac{\partial CN_a}{\partial x_j}\right) \quad (3)$$

Where C is the concentration of the mixture, $C = C_a + C_b$; the concentration of the species "*a*" is C_a. N_a is the mole fraction of species "*a*", $N_a = C_a/C$; D is the diffusion coefficient of the species "*a*".

2.3 Membrane Modeling

The membrane flux equation introduced by Alkhamis et al. [1] is used. The suction rate of the mixture along the surface of the hollow fiber membrane is determined based on the local pressure and concentration [3]. The mass flux through the membrane wall for the species "a" is determined by:

$$J_a = \frac{\ddot{P}_a}{l}\left(p_a^{(1)} - p_a^{(2)}\right) = \frac{\ddot{P}_a}{l}\Delta p_a \qquad (4)$$

Where J_a is the flux of species "a" per unit area, l is the membrane wall thickness, $\ddot{P}_a$ is the permeability of species "a", and $\Delta p_a = \left(p_a^{(1)} - p_a^{(2)}\right)$ is the pressure difference of species "a" through the membrane wall.

The total flux through the membrane wall is presented as:

$$J = J_b + J_a = \Delta p_b \frac{\ddot{P}_b}{l} + \Delta p_a \frac{\ddot{P}_a}{l} \qquad (5)$$

Where J_b is the flux of species "b" per unit area, $\ddot{P}_b$ is the permeability of species "b", and Δp_b the pressure difference of species "b" through the membrane wall.

The selectivity of the membrane is a property that influences the membrane separation performance profoundly. The selectivity of the membrane is defined by the ratio of permeability of species "a" to permeability of species "b":

$\alpha = \ddot{P}_a / \ddot{P}_b$

Equation (5) can be expressed in term of the selectivity:

$$J = \frac{\ddot{P}_b}{l}\left[\Delta p_{tot}\alpha + \Delta p_b(1-\alpha)\right] \qquad (6)$$

Where $\Delta p_{tot} = \Delta p_b + \Delta p_a$ is the total pressure difference through the membrane; $\Delta p_a = N$a Δp_{tot}, is the partial pressure difference for species "a"; therefore, equation (6) can be written as:

$$J = \Delta p_{tot} P_b [N_b(1-\alpha) + \alpha] \quad (7)$$

The suction rate, V_w, across the membrane wall can be expressed in term of molar flux:

$$Vw = J/C \quad (8)$$

Where C is the total concentration of the mixture. Combining equation (7) and equation (8) yields:

$$V_w = \frac{\Delta p_{totP_b}}{C} [N_b(1-\alpha) + \alpha] \quad (9)$$

Therefore, the total pressure difference, mixture total concentration, mass fractions of species and membrane properties influence the suction rate through the membrane wall.

2.4 Boundary Conditions

At the inlet, uniform velocity and concentration profiles are employed. The inlet velocity of each geometry is selected to set values of Reynolds number, $Re = UD_h/v$, 1000, 1500 and 2000. Concentration of 70% CH_4 and 30% CO_2 is set at the inlet for all cases.

At the side boundaries shown with numbers in Figure 2, periodic boundary conditions are applied as an interference with translational motion. Side boundaries are different for the staggered and the inline geometry, as depicted in Figure 2. For the inline geometry, two translational periodic boundary conditions are applied in *y* and *z* cross-flow directions. For the staggered geometry, three translational periodic boundary conditions are applied in the cross-flow directions. In Figure 2, each side is labeled with a number, and it is translationally periodic with other side that label with the same number.

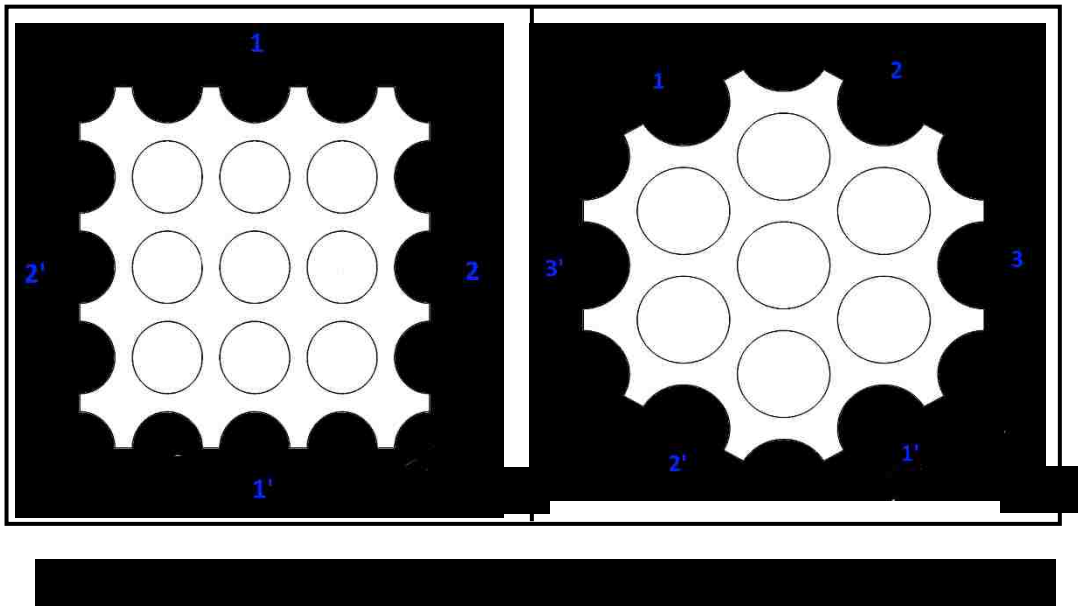

The no-slip condition is applied on membrane surfaces, u = 0. There is a suction along the surface of the membrane and the boundary condition imposed on the velocity

field corresponding to the suction is $u_i n_i =$, where n_i is the out normal of the membrane surface.

The flux condition applied on membrane surface is calculated from conservation of mass:

$$J_a = -D\frac{\partial C_a}{\partial r} = -D\frac{\partial}{\partial r}(CN_a) \tag{11}$$

where *Ca* is the concentration of species "*a*". The derivation of mole fraction of species ''a'' across the membrane surface as provided by [1]

$$\frac{\partial N_a}{\partial r} = \frac{\partial}{\partial r}\left(\frac{C_a}{C_b + C_a}\right) = \frac{1}{C^2}\left(C_b\frac{\partial C_a}{\partial r} - C_a\frac{\partial C_b}{\partial r}\right) \tag{12}$$

By applying equation (11) in mass fraction boundary condition for species "*a*", yields:

$$D\frac{\partial N_a}{\partial r} = \frac{1}{C^2}\left(C_b D\frac{\partial C_a}{\partial r} - C_a D\frac{\partial C_b}{\partial r}\right) = \frac{1}{C^2}(C_a J_b - C_b J_a) \tag{13}$$

From the definition of mole fraction for both species: $N_a = C_a/C$ for species "a"; $N_b = C_b/C$ for species "b", and apply them for the equation (13):

$$D\frac{\partial N_a}{\partial r} = \frac{1}{C}(N_a J_b - N_b J_a) \tag{14}$$

The flux of each species is defined as: $J_a = \Delta p_a P_a$ and $J_b = \Delta p_b P_b$. Substituting flux of each species in equation (14) yields

$$D\frac{\partial N_a}{\partial r} = \frac{1}{C}(N_a \Delta p_b P_b - N_b \Delta p_a P_a) \tag{15}$$

Using the definition of selectivity, $\alpha = P_a/P_b$, the equation (15) becomes:

$$D\frac{\partial N_a}{\partial r} = \frac{P_b \Delta p_{tot}}{C}(1-\alpha) N_b N_a \tag{16}$$

The rejection rate can be defined as the ability of membrane to separate the species of a binary mixture, it can be determined in term of selectivity [5]:

$$R = \frac{\alpha}{\alpha + (1-\alpha)N_b} \tag{17}$$

The mass flux through membrane surface is modeled in term of the rejection rate:

$$-D\frac{\partial C_a}{\partial r} = RV_w C_a \tag{18}$$

For the presented results, the diffusion coefficient for CO_2 is 3.57x10^{-7} m^2/s. The mole fraction of CH_4 at the inlet is chosen 0.7. The permeance of CO_2 is P_{CO_2} = 3.06x10^{-8} $kg/m^2.s\,.Pa$ and the membrane selectivity is $\alpha = P_{CH_4}/P_{CO_2}$ = 0.01415. The total pressure difference across the membrane is selected as Δp_{tot} = 5 MPa.

3. MESH OPTIMIZATION STUDY

Computational fluid dynamics simulations are conducted in three-dimensional hollow fiber module. SolidWorks® is used to generate the computational domain, and ANSYS-MESH V17.1 is used to generate the mesh for the inline and the staggered geometry. A mesh convergence study is designed to prove the mesh independency. The finer mesh is used in regions near surfaces of hollow fiber membranes in order to capture the velocity and the concentration field inside the boundary layer. Figure 3 shows the designed mesh along the membrane surface. Three different mesh sizes are used: 17×10^6 elements 26×10^6 elements, and 37×10^6 elements. The inline geometry with *S/d=1.1* is used in the mesh study for *Re = 1000*. The profile of stream-wise velocity component obtained with three mesh densities are presented in Figure 4b. The profiles are obtained at the cross section located at *L/Dh=30*. Moreover, for three meshes, CH_4 concentration along the hollow fiber membrane at *L/Dh=30* are presented in Figure 4a. Concentration profiles are presented for the hollow fiber membrane located at the center.

Figure 4 clearly demonstrate that the velocity field in the bulk region and the concentration distribution along the surface of the membrane are nearly the same for mesh density of 26 million and 37 million elements. The mesh density of 26×10^6 elements is sufficient to attain spatial convergence in this geometry. It is important to note that each geometry has different length and different hydraulic diameter; requiring a different number of total elements. Table 2 shows the number of elements for each case. The length of the computational domain has also been adjusted with values of Re or flow rates applied. Similar refinement level is used in all geometries.

	Inline		Staggered	
	S/d = 1.25	**S/d = 1.1**	**S/d =1.25**	**S/d = 1.1**
L/D_h	40	40	75	75
Elements number (M)	47.8	26	56.5	25.6

Table 2: Elements number for each case.

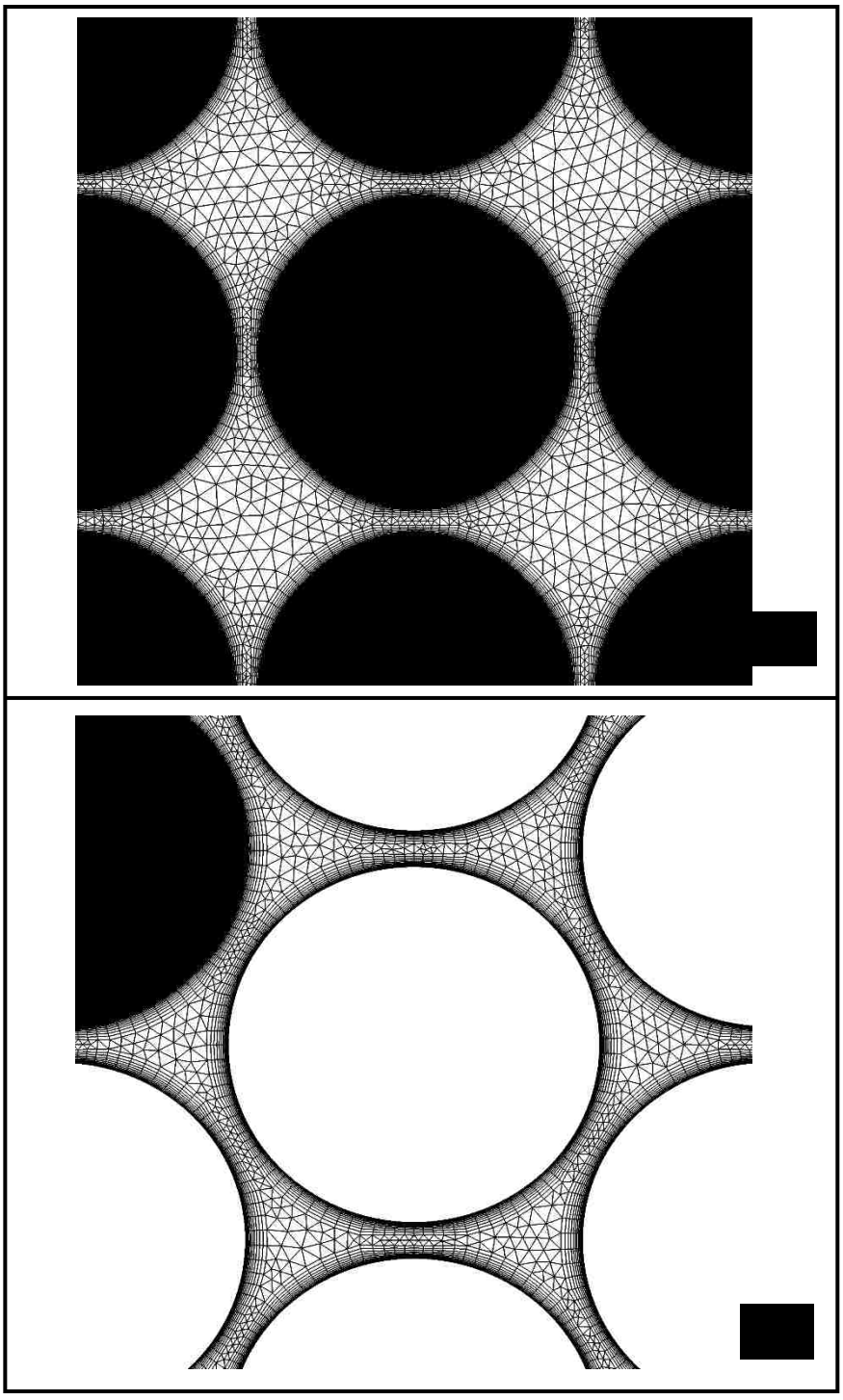

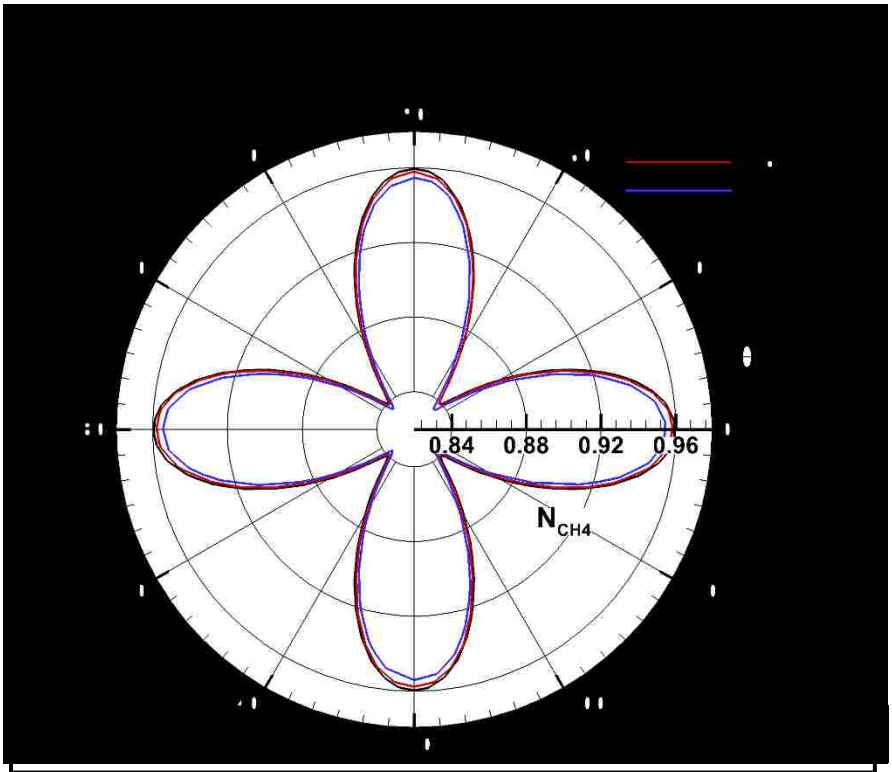
0.84
0.88
0.92
0.96
N_{CH4}

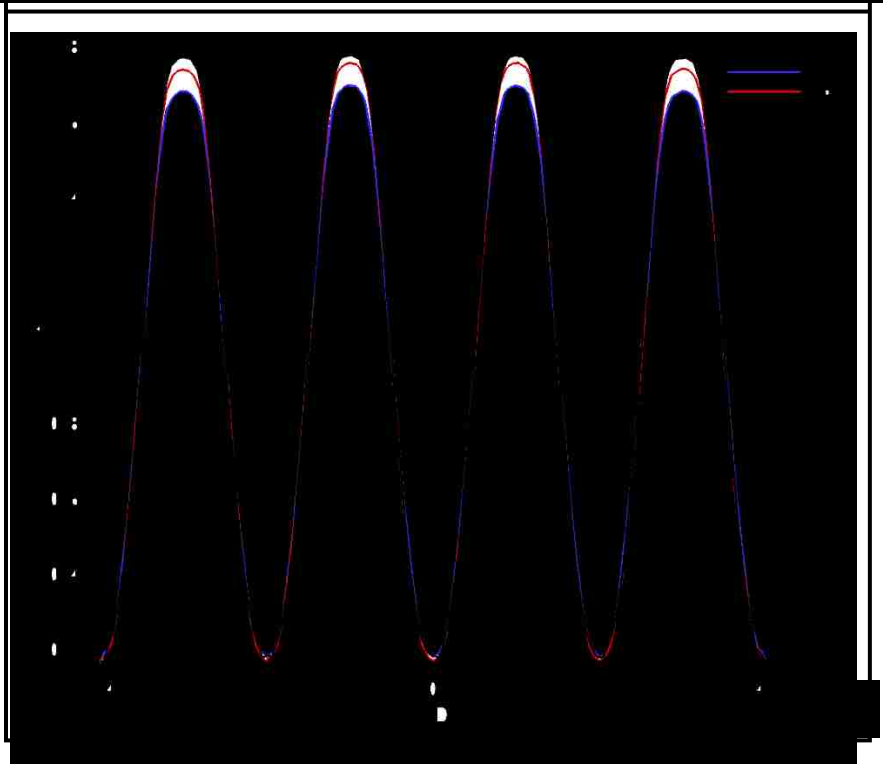

4. RESULTS

Simulations are conducted to study steady state three-dimensional flow in a gas separation module containing hollow fiber membranes. Axial flow of CH_4-CO_2 binary mixture is considered in the inline and the staggered geometry with a spacing of *S/d = 1.1* and *S/d = 1.25* at *Re = 1000, 1500,* and *2000*.

Figure 5 shows contours of the stream-wise component of velocity, the magnitude of vorticity, and CH_4 concentration in the inline and staggered geometry for *Re = 2000* and *S/d = 1.1*. Images are acquired at the planes as shown in Figure 5a and 5b for the corresponding geometry. In the inline geometry, the image plane is chosen to be at the center of the closed gap between the center column and the column adjacent to it at (Z/D_h *= 1*). Image plane for the staggered geometry is chosen to be at the center of the computational domain, which cuts through the centered membrane.

The steam-wise velocity components are normalized with the inlet velocity. Figure 5c depicts the contour of the stream-wise component velocity in the inline geometry while Figure 5d from depicts the velocity contour in the staggered geometry. Velocity contours in both geometry show flow in both geometries are hydrodynamically developed away from the inlet. For the selected cross-sections, normalized velocity is higher in the inline case than that in staggered case. This is because staggered inherently has 6six narrow gap which causes more surface friction and relatively higher normalized velocities. It is observed that for both cases, maximum velocity occurs at the center of the region between two adjusted fibers, where the boundary layer thickness extends; this is because of the absence of the shear stress.

Figure 5e and Figure 5f show contours of the vorticity magnitude for each geometry for *Re = 2000* and *S/d = 1.1*. It is shown that regions with the wider gap between fibers have lower vorticity than regions with narrow gaps; resulting from low friction and the low velocity in regions with wider gaps. That illustrates low momentum mixing occurs at these regions. Also, these figures are showing that the flow is fully developed for both cases, where the vorticity profile is not changing in the stream-wise direction. Overall, the velocity and vorticity contours are not changing in the flow direction away from the inlet; indicating that the momentum layer is fully developed.

Contours of CH_4 concentration for the selected planes are shown in Figure 5g and Figure 5h for the inline and the staggered geometry, respectively. It is shown that CH_4 concentration field is still developing due to the active CO_2 passage through the hollow fiber membranes. Moreover, it is observed that the mixture is gradually becoming richer in CH_4 away from the inlet, toward the outlet. This indicates that hollow fiber membranes are performing properly by preferentially passing CO_2 and rejecting CH_4. It is shown for both cases that the higher CH_4 concentration region coincides with high vorticity regions in the bulk (i.e. wider regions have lower CH_4 concentration than that in the narrow regions). The inline geometry has higher CH_4 concentration than that in the staggered case. In the inline geometry, it takes longer time for the mixture to go from the inlet to the outlet compared to the staggered geometry, which provides the mixture more residence time for CO_2 passing through the membrane.

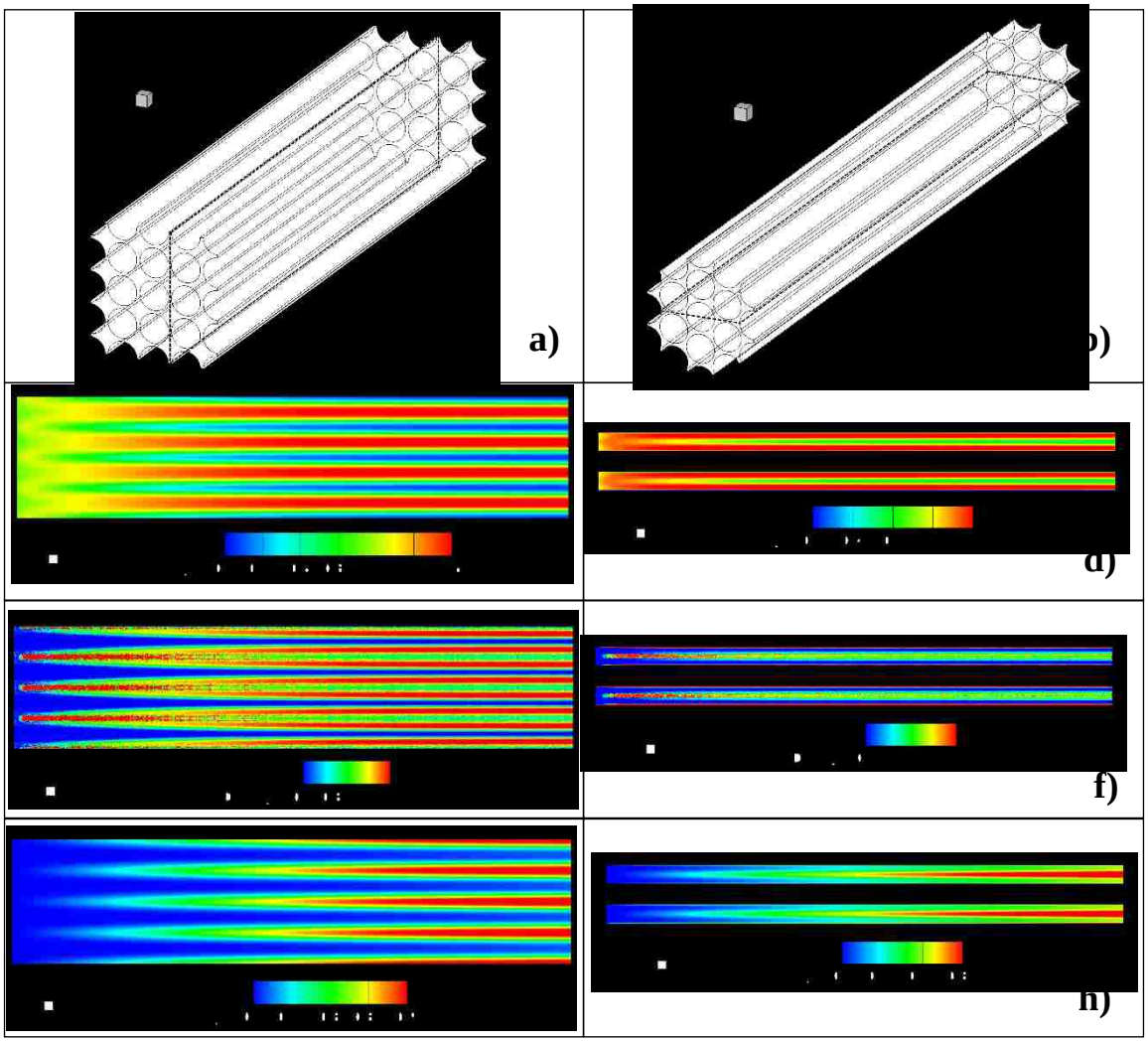
a)
d)
f)
h)

Figure 6 depicts contours of the stream-wise component of the velocity at a selected cross-section. Images are acquired for $Re = 2000$ and $S/d = 1.25$ and $S/d = 1.1$ for the inline and staggered arrangements. Figures 6a and 6c are for inline geometries, and Figures 6b and 6-d are for staggered geometries. The cross section is selected at $X/D_h = 30$ for inline cases and $X/D_h = 60$ for the staggered cases. The velocity is normalized with the average inlet velocity. Figure 6 proves that the periodic boundary conditions are working properly for the system, where velocity around each fiber is identical with other fibers. It shows that narrow gaps tend to have lower normalized velocity magnitude than that in the wider gaps because the fluid tends to move in the wider regions where lower resistance exists. Also, it is observed that six higher velocity regions are surrounding the membranes, while there are four in the inline cases. As a comparison for any arrangements with two different spacing, there is a glaring contrast between the wide (high-speed regions) and the narrow (low fluid speed regions) in both geometries. The difference in speeds in high and low-speed regions is increasing as the spacing between membrane surfaces is decreased. This has profound influence in hollow fiber membrane flux performance in these high and low-speed regions.

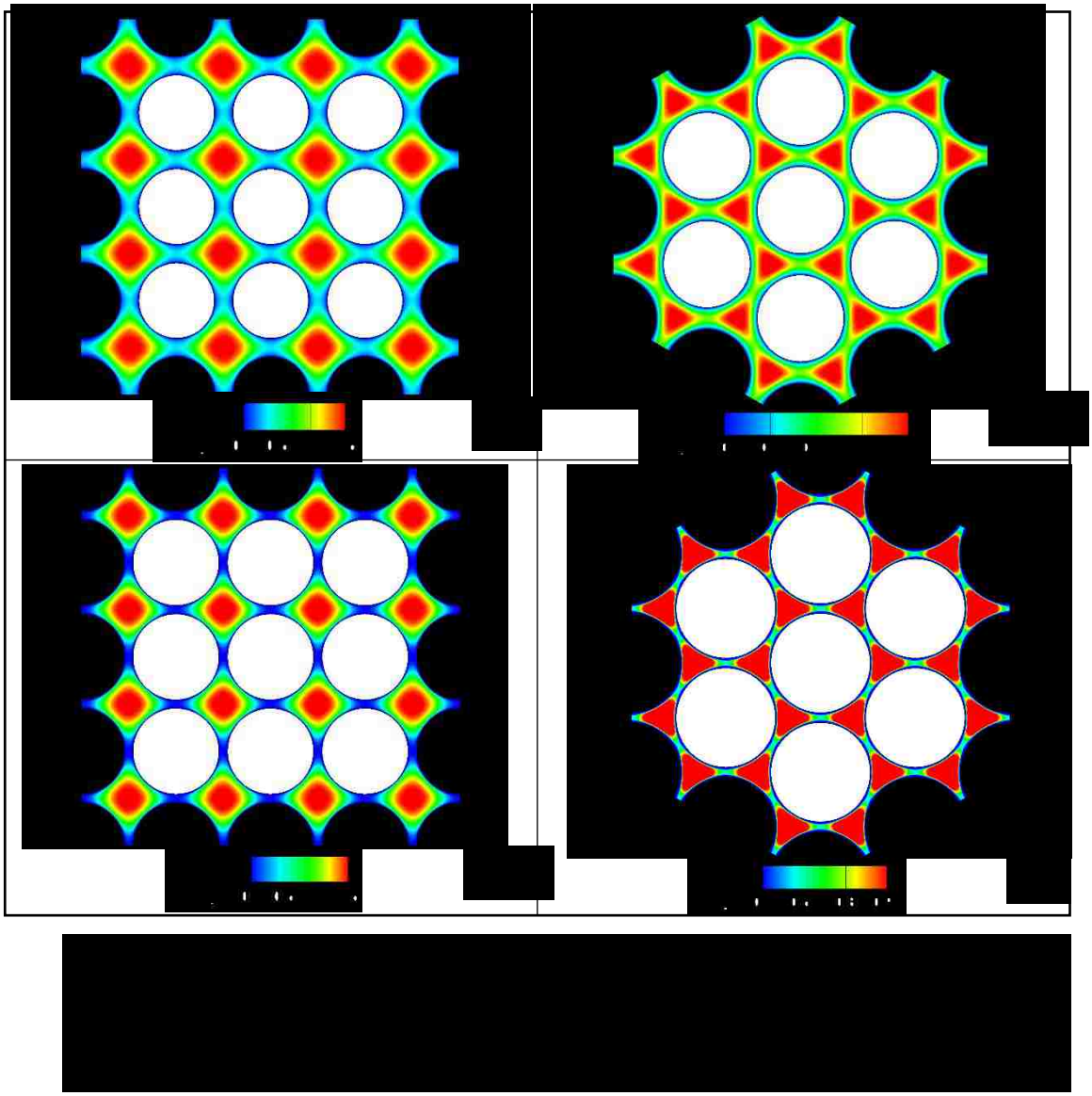

Contours of the normalized vorticity magnitude are shown in Figure 7 for *Re = 2000.* Contours are obtained for the inline and the staggered geometries with *S/d = 1.25* and *S/d = 1.1.* Figures 7a and 7c are for the inline geometries, and Figures 7b and 7d are for staggered geometries. The cross section for the contour plane is selected at $X/D_h = 30$ and $X/D_h = 60$ for the inline and staggered cases, respectively. The vorticity is normalized with hydraulic diameter D_h over the inlet velocity U_{inlet}. As a comparison between the two arrangements, it shows that, for one spacing, the vortical activity decays faster in the staggered geometry than that in the inline geometry. Also, i decays faster as the spacing between membranes becomes tighter. The lowest level of vorticity obtained inside the bulk, further away from boundary layers where high speed is obtained. Boundary layers in the narrow gap region have lower vorticity than those in the wider region because the boundary layer thickness is larger in the wider gap than the narrow gap. For the staggered case, contours show patterns of six high and six low vorticity regions around each hollow fiber while patterns of four high and low regions exist in the inline geometry, as illustrated in Figure 7.

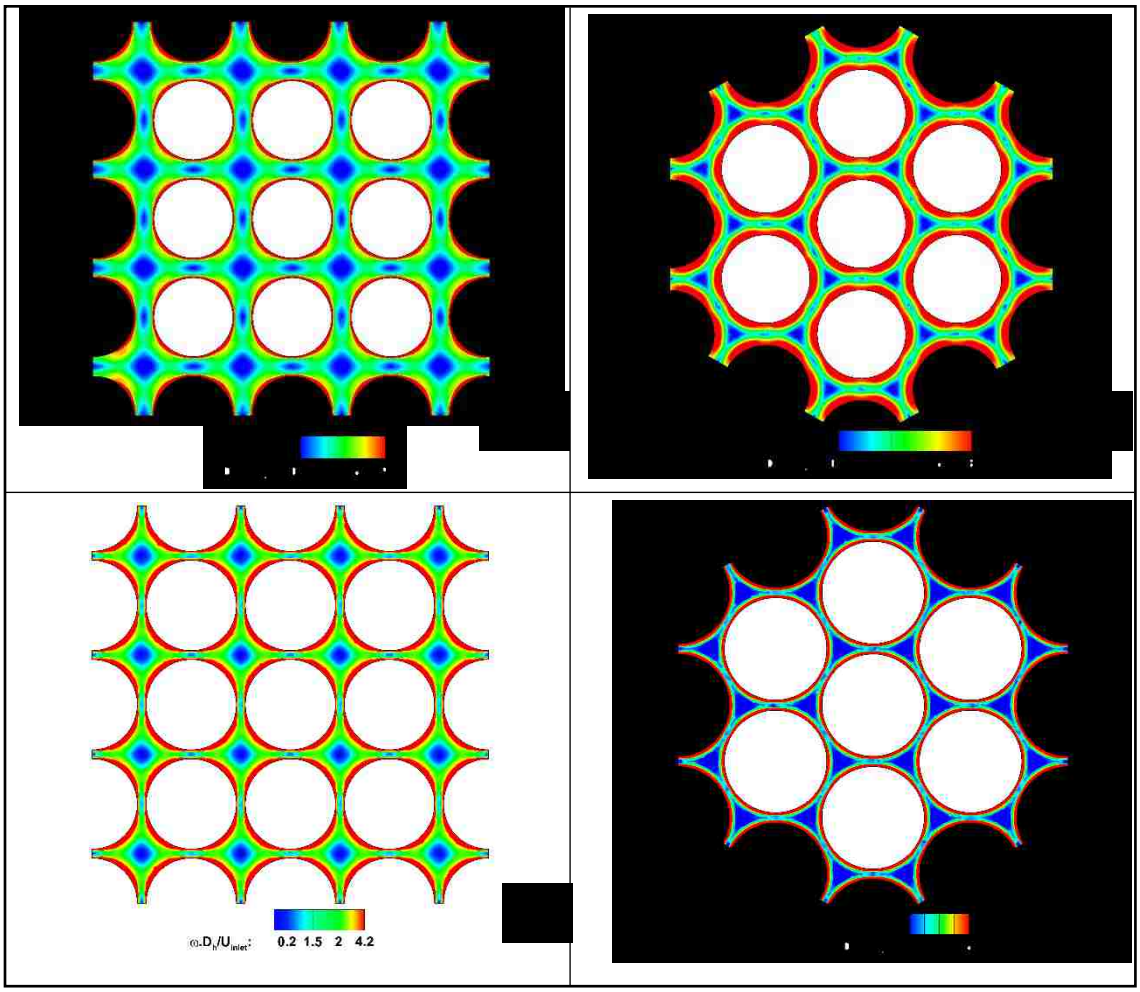
ω.D_h/U_inlet:
0.2 1.5 2 4.2

Contours of CH_4 concentration are shown in Figure 8 at the cross-section $X = 30\ D_h$ for the inline geometry and at $X = 60\ D_h$ for the staggered geometry respectively for $Re = 2000$ and $S/d = 1.25$ and 1.1. Figures 8a and 8c show images for the inline configurations with two values of spacing while Figures 8b and 8d depict images for staggered configurations. Following vorticity patterns in the bulk region, regions of the narrow gap have a higher concentration than that those of wide gap. This is attributed to the fact that regions in the wider gap have lower vorticity magnitude. Since the residence time of the fluid in the module is much shorter in the staggered geometries, area averaged CH_4 concentration level is lower than that in the inline case for the same value of spacing and Reynolds number, as shown in Figure 8. CO_2 in the module with the inline configuration of hollow fibers has significantly more time to pass through the membrane and thus the mixture becomes richer in CH4 toward the outlet compared to the staggered module. With these result alone we can't conclude that the inline geometry performs better that the staggered geometry. The combination of Sherwood number and the pressure drop inside the module will determine the performance of these modules. Performance comparison of modules with different configurations will be discussed in detail below.

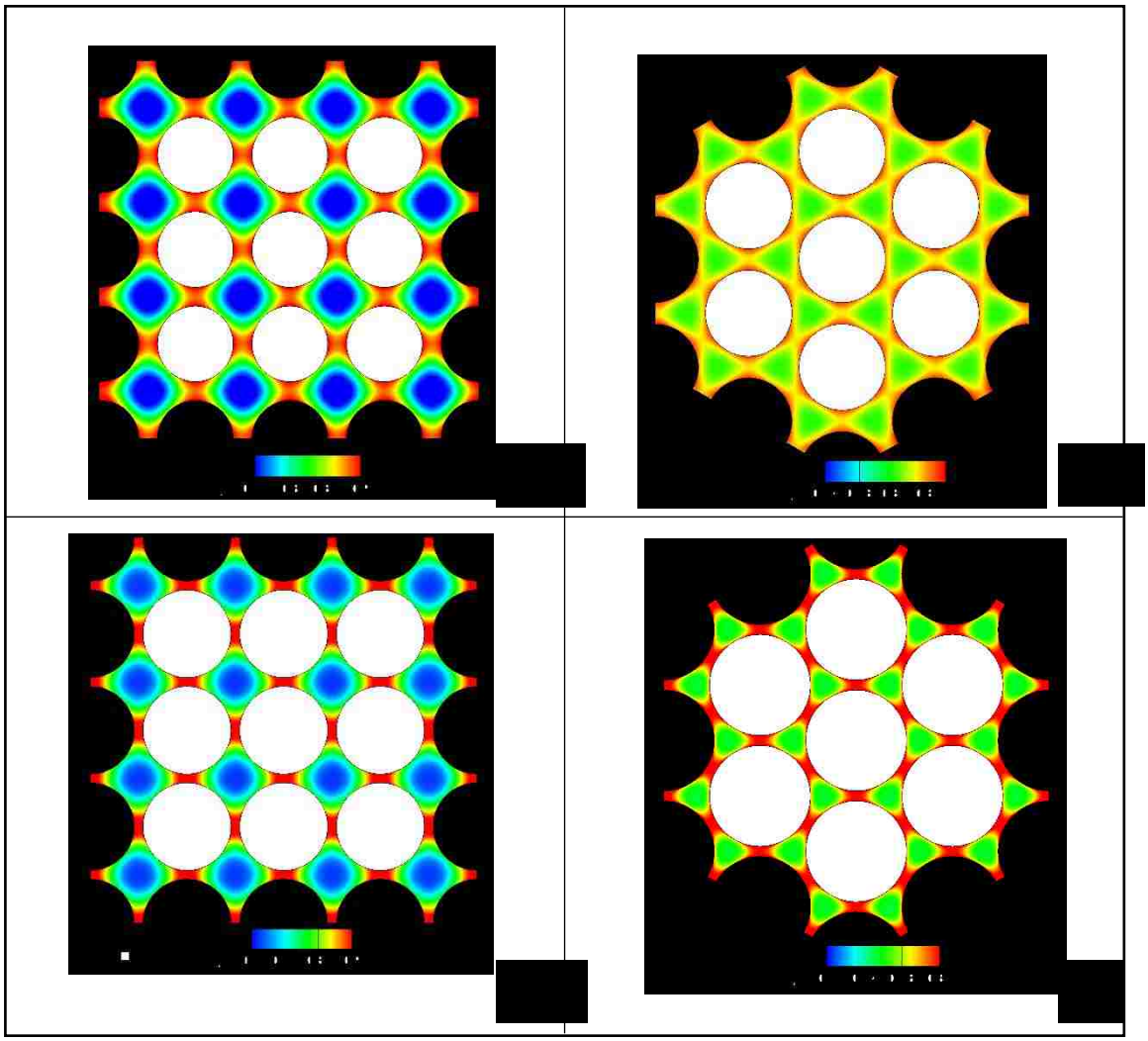

Next, properties of the surface of hollow fibers will be presented and discussed. Figure 9 illustrates profiles of CH_4 concentration and the suction rate for the inline and staggered arrangements with *S/d = 1.1* for *Re = 1000, 1500,* and *2000.* Profiles are plotted as a function of azimuthal angle, θ, along with the hollow fiber membrane surface at a cross-section of *30* D_h for the inline geometry and *60* D_h for the staggered geometry. The hollow fiber at the center of the cross-section is selected for the profiles. The suction rate is normalized with P_{CO2} and ΔP. Figure 9a and Figure 9b show concertation profiles for the inline and the staggered arrangements. The inline case has four narrow regions, while the staggered case has six narrow regions around each hollow fiber. These regions have higher concentration because of low vorticity. For both cases at low flow rates, a higher level of concentration is observed due to lower residence time, as discussed earlier. .. As a comparison between inline and staggered concentration profiles, inline cases have higher levels of CH_4 than that in the staggered case corresponds to the same value of Reynolds number. Again, this attributed to the lower residence time in the staggered geometry compared to that in the inline geometry. The magnitude of the concentration polarization in each module should be judged comparing the level of concentration along the surface of the membrane and in the bulk region of the feed channel.

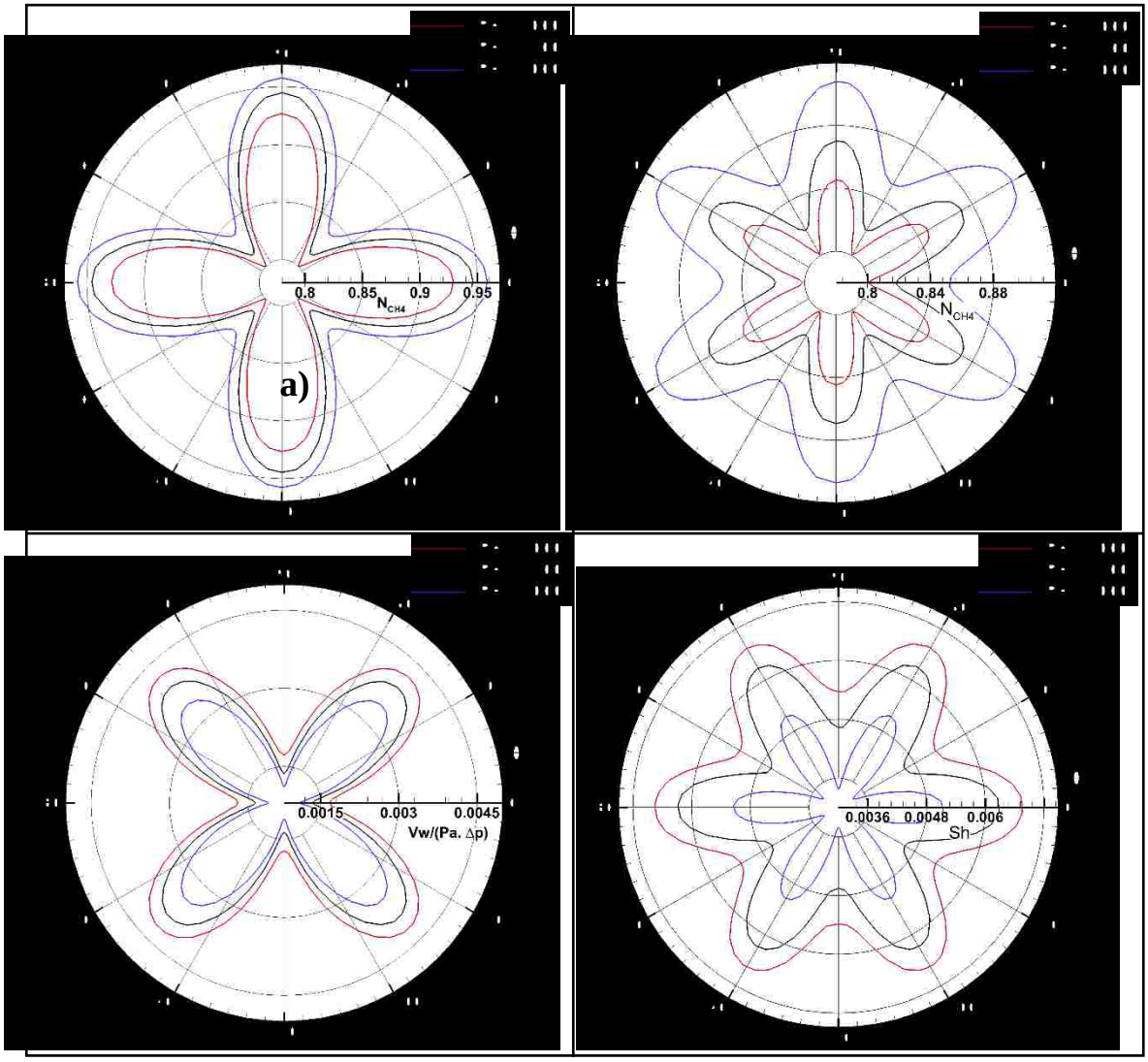
a)
0.8
0.85
0.9
0.95
N_{CH4}
0.8
0.84
0.88
N_{CH4}
0.0015
0.003
0.0045
Vw/(Pa. Δp)
0.0036
0.0048
0.006
Sh

Figures 9c and 9d show the normalized suction rate for the inline and the staggered arrangements at the selected cross-section of the centered membrane. Similar to the pattern of azimuthal concentration profiles, the suction rates depict repeated patterns of six high and low suction rate regions along the hollow fiber in the staggered arrangement and four repeated high and low regions in the inline arrangement, as shown in Figure 9. The maximum suctions of CO_2 occur in the membrane in the angle toward the wide-gap regions. The profiles show that the suction rate increases with increasing Reynolds number. It is also showing that higher suction rate regions coincide with higher CH_4 concentration regions. The Higher rate of CO_2 passage through the membrane make the mixture richer in CH_4. Hollow fiber membranes in the staggered configuration have higher suction rate levels than those in the inline configuration at the same value of Reynolds number.

Sherwood Number Calculations

Sherwood number is defined as the ratio of the convective to diffusive mass transfer and measures the performance of the hollow fiber membrane. Sherwood number can be calculated by:

$$Sh = \frac{h_m D_h}{D} \tag{19}$$

Where *Sh* is the local Sherwood number, D_h is the hydraulic dimeter, *D* is the binary diffusion coefficient of the mixture h_m is the mass transfer coefficient and can be calculated by:

$$h_m = \frac{-D\frac{\partial C_a}{\partial y}}{(C_m - C_w)} \tag{20}$$

Where C_m is the bulk concentration of the species "*a*", c_w is the concentration of species "*a*" at the membrane surface.

Figure 10 illustrates profiles of the Sherwood number along with the surface of the centered hollow fiber membrane as a function of the azimuthal angle, Θ. Profiles are plotted for the membrane in the inline and the staggered arrangements at *Re =1000, 1500,* and *2000* for *S/d = 1.1*. The profiles are determined at cross-section *30* D_h for the inline geometry and at *60* D_h for the staggered geometry. Profiles show that Sherwood number follows the vorticity structure, where it is higher on membrane surface at the angles in the wide regions. These regions have a higher suction rate of CO_2 across the membrane. Sherwood number of the hollow fiber in the staggered arrangement is higher than that in the inline case at the same value of Reynolds number. In both geometry higher values of Sherwood number in the wide-gap regions compared to low-gap regions; leads patterns of six high and low Sherwood number along with the surface of the hollow fiber in the staggered region and the pattern of four high and low regions in the inline geometry. In both geometries, it is shown overall the Sherwood number is higher in the modules with hollow fibers spaced with tighter configuration.

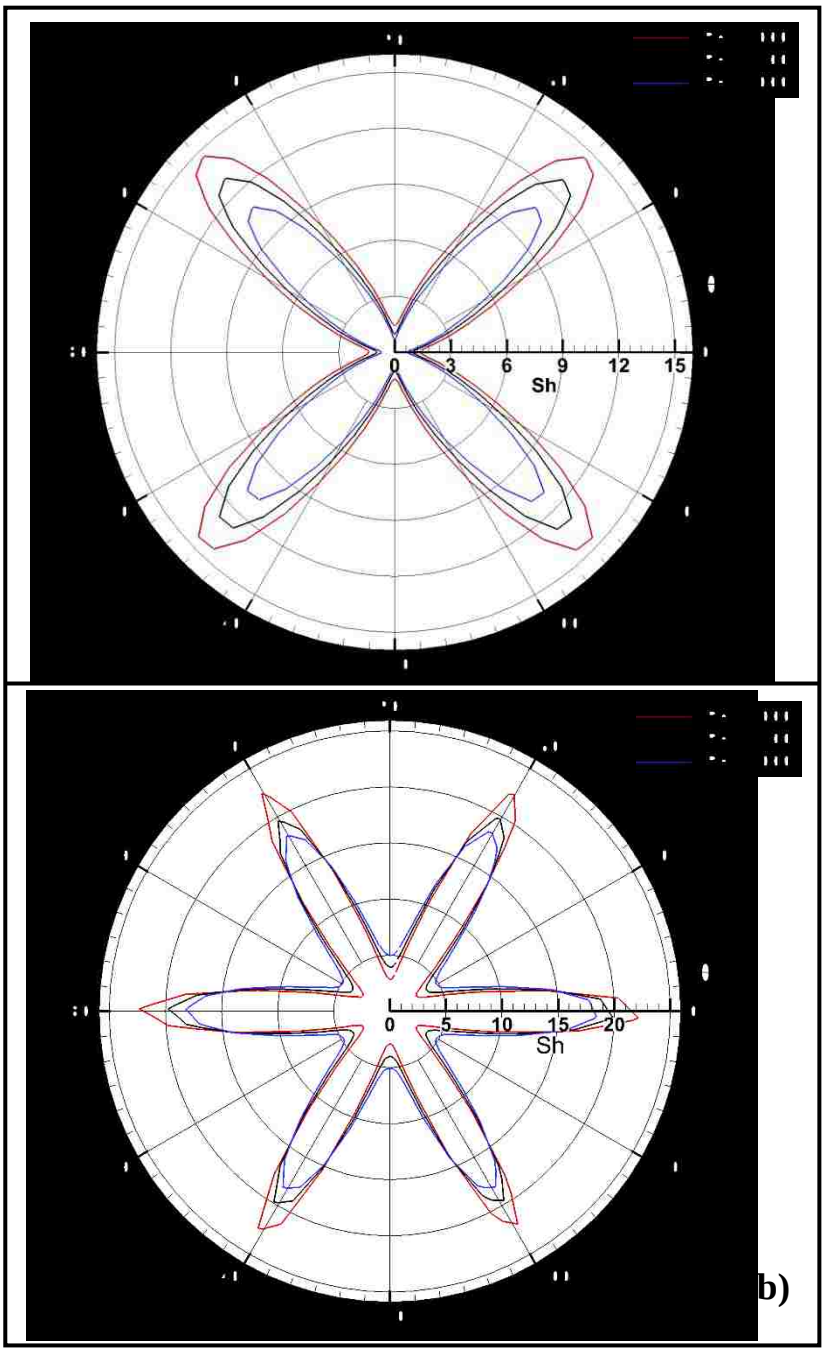

b)

Profiles of averaged Sherwood number are plotted in Figure 11 as a function of X/D_h for the inline and staggered arrangements. Average value of Sherwood number is determined at each cross-section by area averaging. Figures 11a and 11c depict profiles for the inline arrangements with *S/d = 1.25* and *S/d = 1.1* and Figures 11b and 11d depict profiles for staggered arrangements with *S/d = 1.25* and *S/d = 1.1*. Profiles are obtained for *Re = 1000, 1500,* and *2000*. It is important to note that area-averaged Sherwood number asymptote a constant value away from the inlet, as shown in Figure 11. In both geometries, Sherwood number increases with increasing Reynolds number; this is an indication of the higher rate of CO_2 passage as modules operates with higher Reynolds number. In each geometry, the Sherwood number is greater in the module with hollow fibers spaced with a wider gap. Hollow fiber with the staggered arrangement has a greater value of Sherwood number compared to those in the inline arrangement at the same Re, suggesting that staggered geometry performs better than inline geometry for the value of same spacing and Reynolds number.

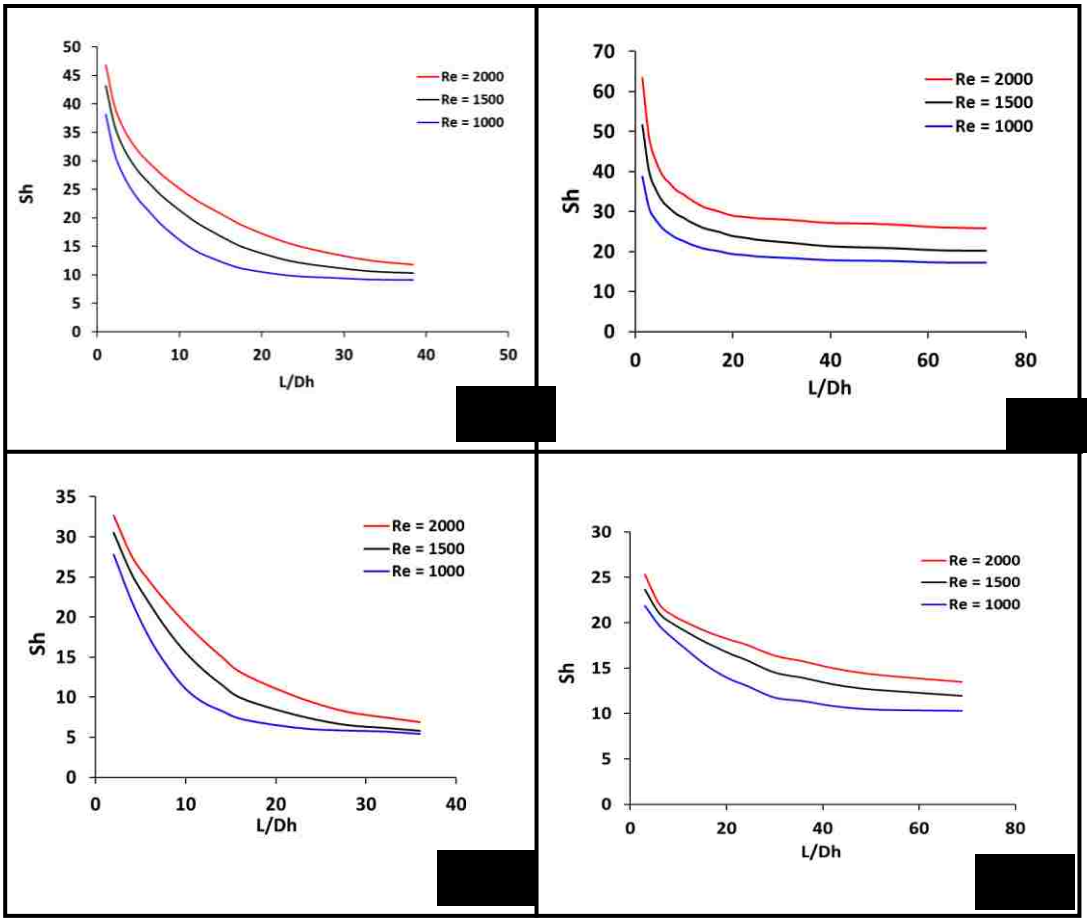

[redacted]

Table 3 depicts the averaged Sherwood number, $\overline{Sh}$, for the inline and staggered arrangements for Reynolds number of 1000, 1500 and 2000 and for *S/d = 1.25* and *1.1*. The value of $\overline{Sh}$ in each geometry is determined for the asymptotic value of the Sherwood number away from the inlet and represent the overall average value of the module. .It is shown that averaged Sherwood number increases as the Reynolds number increases in all geometries. Sherwood number is higher for the hollow fibers in the staggered arrangement compared to those in the inline arrangement at the same spacing and for the same value of Re. It is also depicted that Sherwood number of the fiber in tighter spacing is lower in both geometry at the same value of Reynold number.

Re	**S/d = 1.25**		**S/d = 1.1**	
	inline	**Staggered**	**inline**	**Staggered**
1000	9.50	17.59	5.83	10.55
1500	11.46	20.79	6.68	12.83
2000	13.92	26.65	8.34	14.53

Table 3: Averaged Sherwood number along the hollow fiber membrane surface for inline and staggered cases at different Re and S/d.

The friction factor of flow inside the module is determined from the pressure drop across the module as

$$fr = \frac{2D_h}{\rho {U_{inlet}}^2} \frac{\Delta P}{L} \tag{21}$$

Where ΔP is the pressure drop in the module. L is the length of module across which the pressure drop is determined; D_h is the hydraulic diameter; U_{inlet} is the average velocity at the inlet. Table 4 shows the calculated averaged friction factor for the inline and staggered arrangements for Reynolds number of 1000, 1500 and 2000 and for *S/d = 1.25* and *1.1*.. The friction factor will measure the energy loss for the separation by membrane system. Table 4 show that the pressure drop in the staggered case is higher than that in the inline case at the same value of Reynolds number and with the same spacing. It shows that the friction factor increases with the increase of spacing; this is valid for both the inline and the staggered geometry. Moreover, it shows that friction factor is nearly independent of Re for the range of flow rates considered here.

Re	S/d = 1.25		S/d = 1.1	
	inline	Staggered	inline	Staggered
1000	0.033	0.043	0.012	0.029
1500	0.024	0.031	0.009	0.021
2000	0.024	0.031	0.008	0.016

Table 4: Friction factor along the hollow fiber membrane surface for inline and staggered cases at different Re and S/d.

The coefficient of performance (COP) is defined by:

$$\text{COP} = \frac{Sh_s/Sh_i}{(fr_s/fr_i)^{1/3}} \tag{22}$$

where Sh_s and Sh_i are the average value of the Sherwood number of the module containing hollow fibers with the staggered and the inline arrangements, respectively. fr_s and fr_i are the friction factors of modules containing hollow fibers with the staggered and the inline arrangements, respectively. . COP compares the flux performance of modules with different arrangements operating with the same pumping power.

Table 5 shows the COP for different values of Reynolds number and spacing. It is important to note that all COP is greater than unity for both spacings at all values of Re, demonstrating that the staggered arrangement of the hollow fiber is performing better for separation CO_2 fro CH_4.It is also shown that COP is insensitive to Re for both spacings; suggesting that flux performance improves the same level as Re is increased.

Re	**S/d = 1.25**	**S/d = 1.1**
1000	1.70	1.35
1500	1.67	1.47
2000	1.75	1.37

Table 5: Coefficient of performance values at different Re and S/d.

5. CONCLUSIONS

Numerical simulations are conducted to study steady flow and mass transport in three-dimensional gas separation modules containing arrays of reverse osmosis hollow fiber membranes. Hollow fibers are arranged with an inline and a staggered configuration. Two spacing of hollow fibers, *S/d = 1.25* and *1.1*, are considered in this study. The fluid, a binary mixture of CH_4 and CO_2, flows in a direction parallel to the membrane axis. Flow inside the feed of hollow fiber membrane module is laminar. Equations governing fluid motion and mass transport in the module, Navier-Stokes equation and mass transport equations, are solved for a range of Reynolds number between 1000 and 2000. Flow is fully developed away from the inlet development length differs in the inline and staggered cases at a given flow rate. Concentration layer continues to develop throughout the computational domain and the mixture becomes richer in methane further away from the inlet. It shows that the membrane functions properly by letting more CO_2 passage. Concentration distribution inside the module is directly influenced by the level of momentum mixing, as a result regions of low concentration coincides with regions of low vertical activities in modules with the inline and the staggered configuration. The averaged CH_4 concentration is higher in the inline cases than that in the staggered cases at a given flow rate. This is due to the fact the residence time of the fluid is higher in the inline geometry, and thus there is more time for passage of CO_2 through the membrane as the mixture passes through the module. The suction rate of CO_2 on membrane surfaces profiles are calculated for all cases considered. Results reveal that the suction rate is higher in the wide gap region between hollow fibers where higher fluid speed is obtained. Higher fluid

speed regions also coincide with higher vorticity and lower concentration regions. The distribution of suction rates along the hollow fibers at a given cross-sections follows the pattern around hollow fibers. Sherwood number of hollow fibers membrane is determined inside the module and illustrates a similar pattern of suction rates. Sherwood number is greater in the staggered geometry compare to that in the inline geometry for the same value of spacing and Reynolds number. Sherwood number in both geometry increases as Reynold number It is also shown that Sherwood decreases as the spacing between hollow fibers become tighter. The coefficient of performance or merit number is calculated to compare module flux performance between the staggered and the inline geometry. The module with staggered arrangement performs much better than the module with the inline arrangement at all flow rates. It is noticed that performance hardly changes with Reynolds number for the range of flow rates considered. Mass flow rate of CO_2 passing across the membrane surfaces is presented for different values of Reynolds number and spacing. It is higher in the staggered geometries than in the inline geometries; confirming the better performance of staggered geometries. This study will aid in designing the reverse osmosis gas separation modules. Further study will be needed to better understand the influence of hollow fiber arrangement, spacing, and shape on the flux performance of these modules.

6. BIBLIOGRAPHY

[1] N. Alkhamis, D.E. Oztekin, A.E. Anqi, A. Alsaiari, A. Oztekin, Gas Separation Using a Membrane, ASME 2013 Int. Mech. Eng. Congr. Expo. Am. Soc. Mech. Eng. (2013) V07AT08A039-V007AT008A039.

[2] N. Alkhamis, D.E. Oztekin, A.E. Anqi, A. Alsaiari, A. Oztekin, Numerical study of gas separation using a membrane, Int. J. Heat Mass Transf. 80 (2015) 835–843.

[3] M. Alrehili, M. Usta, N. Alkhamis, A.E. Anqi, A. Oztekin, Flows past arrays of hollow fiber membranes - Gas separation, Int. J. Heat Mass Transf. 97 (2016) 400–411.

[4] A.E. Anqi, N. Alkhamis, A. Oztekin, Computational study of desalination by reverse osmosis - Three-dimensional analyses, Desalination. 388 (2016) 38–49.

[5] Baker, R. W. (2012). Membrane Technology and Applications (3). Somerset, GB: Wiley. Retrieved from http://www.ebrary.com

[6] Energy information administration of US Department of Energy., International energy outlook 2016-Natural gas, Int. Energy Outlook 2016. 2016 (2016) 37–60.

[7] G.A. Fimbres-Weihs, D.E. Wiley, Numerical study of mass transfer in three-dimensional spacer-filled narrow channels with steady flow, J. Memb. Sci. 306 (2007) 228–243.

[8] H.A. Hubbard, Heat Transfer to Longitudinal Laminar, J. Heat Transfer. (1961) 415–422.

[9] S.K. Karode, A. Kumar, Flow visualization through spacer filled channels by computational fluid dynamics I. Pressure drop and shear rate calculations for flat sheet geometry, J. Memb. Sci. 193 (2001) 69–84.

[10] T. Katoh, M. Tokumura, H. Yoshikawa, Y. Kawase, Dynamic simulation of multicomponent gas separation by hollow-fiber membrane module: Nonideal mixing flows in permeate and residue sides using the tanks-in-series model, Sep. Purif. Technol. 76 (2011) 362–372.

[12] C.P. Koutsou, A.J. Karabelas, A novel retentate spacer geometry for improved spiral wound membrane (SWM) module performance, J. Memb. Sci. 488 (2015) 129–142.

[13] B. Marcos, C. Moresoli, J. Skorepova, B. Vaughan, CFD modeling of a transient

hollow fiber ultrafiltration system for protein concentration, J. Memb. Sci. 337 (2009) 136–144.

[14] S.M. Mojab, A. Pollard, J.G. Pharoah, S.B. Beale, E.S. Hanff, Unsteady laminar to turbulent flow in a spacer-filled channel, Flow, Turbul. Combust. 92 (2014) 563–577.

[15] H. Sadeghifar, N. Djilali, M. Bahrami, A compact closed-form Nusselt formula for laminar longitudinal flow between rectangular / square arrays of parallel cylinders with unequal row temperatures, Int. J. Therm. Sci. 100 (2016) 248–254.

[16] A. Saeed, R. Vuthaluru, H.B. Vuthaluru, Impact of Feed Spacer Filament Spacing on Mass Transport and Fouling Propensities of RO Membrane Surfaces, Chem. Eng. Commun. 202 (2015) 634–646.

[17] A. Saeed, R. Vuthaluru, Y. Yang, H.B. Vuthaluru, Effect of feed spacer arrangement on flow dynamics through spacer filled membranes, Desalination. 285 (2012) 163–169.

[18] M. Shakaib, S.M.F. Hasani, M. Mahmood, CFD modeling for flow and mass transfer in spacer-obstructed membrane feed channels, J. Memb. Sci. 326 (2009) 270–284.

[19] U.S. Energy Information Administration, International Energy Outlook 2016, 2016.

[20] F. Vinther, M. Pinelo, M. Br??ns, G. Jonsson, A.S. Meyer, Predicting optimal back-shock times in ultrafiltration hollow fibre modules through path-lines, J. Memb. Sci. 470 (2014) 275–293.

[21] B. Wetenhall, J.M. Race, M.J. Downie, The Effect of CO_2 Purity on the Development of Pipeline Networks for Carbon Capture and Storage Schemes, Int. J. Greenh. Gas Control. 30 (2014) 197–211.

7. VITA

Alaa K. Hakim was born On July 15th, 1990 in Ad Diwaniyah city, Iraq. He is married and has two children. In 2007, Alaa was accepted to enter the college of engineering / Al Qadisiyah University. In 2011, he graduated with Bachelor degree; he ranked (1) among the graduate student in the mechanical engineering department. Alaa worked as a mechanical construction supervisor engineer until 2013, and then he was employed as a supervisor-drilling engineer in the department of oil, Iraq. He received many certificates from different authorities and academic stuff and in his work fields. In 2013, Alaa was nominated for a full sponsored scholarship by The Higher Committee for Education Development in Iraq / Office of Prime Minister to pursue Master of Science degree in mechanical engineering. He joined the program in mechanical engineering at Lehigh University, the United State of America in fall, 2015. He received his Master of Science degree in May 2017.